Biosensors and Bioelectronics 85 (2016) 261–266

Contents lists available at ScienceDirect

Biosensors and Bioelectronics

journal homepage: www.elsevier.com/locate/bios

A photoacoustic immunoassay for biomarker detection

Yunfei Zhao [a], Mingfeng Cao [b], John F. McClelland [c], Zengyi Shao [b], Meng Lu [a,d,*]

[a] Department of Electrical and Computer Engineering, Iowa State University, Ames, IA 50011, USA
[b] Department of Chemical and Biomolecule Engineering, Iowa State University, Ames, IA 50011, USA
[c] MTEC Photoacoustics Inc., 3507 Oakland St. Ames, IA 50014, USA
[d] Department of Mechanical Engineering, Iowa State University, Ames, IA 50011, USA

ARTICLE INFO

Article history:
Received 12 March 2016
Received in revised form
28 April 2016
Accepted 7 May 2016
Available online 9 May 2016

Keywords:
Biomarker
Photoacoustics
Immunoassay
Surface plasmon resonance
ELISA
Nanoparticle
Human interleukin-8

ABSTRACT

Challenges in protein biomarker analysis include insufficient sensitivity for detecting low-abundance biomarkers, poor measurement reproducibility, and the high costs and large footprints of detection systems. To address these issues, a new detection modality was developed for analyzing protein biomarkers based on the plasmon-enhanced photoacoustic (PA) effect. The detection modality employed a heterogeneous immunoassay scheme and used gold nanoparticles (AuNPs) as the signal reporter. Due to their localized plasmon resonance, AuNPs can strongly interact with intensity-modulated laser excitation and generate strong PA signals, which are subsequently sensed and quantified using a microphone. As an example, the performance of the PA immunoassay was evaluated by detecting the human interleukin 8 chemokine. The PA immunoassay provided approximately 143 × lower limit of detection (LOD) than observed with the gold standard enzyme-linked immunosorbent assay – a decrease from 23 pg/mL to 0.16 pg/mL. In addition to the significant performance improvement in terms of the LOD, the PA immunoassay also offers advantages in terms of compatibility with low-cost instruments and the long-term stability of assay results.

© 2016 Elsevier B.V. All rights reserved.

1. Introduction

The ability to detect and quantify disease-related biomarkers at trace concentrations enables diagnosis of the corresponding disease at an early stage (Fan et al., 2008; Hanash et al., 2011; Ludwig and Weinstein, 2005; Rhea and Molinaro, 2011). The predominant methods used for biomarker detection rely on immunoassays, which enable the measurement of protein-biomarker concentrations in a complex solution with antibodies. Immunoassays can target specific biomarkers and measure their concentrations with very high sensitivity and specificity. Most immunoassays employ some type of labeling materials, such as enzymes, fluorescent dyes, magnetorotational labels, or radioactive isotopes, to generate a detectable signal (Gan and Patel, 2013; Hecht et al., 2011; Huang et al., 2011; Lequin, 2005; Voller et al., 1978; Yingyongnarongkul et al., 2003). Among the various types of immunoassays, enzyme-linked immunosorbent assays (ELISAs) are considered the gold standard, where enzymatic tags are used to generate colorimetric signals in liquid substrates. Chemiluminescence- and fluorescence-based immunoassays have become popular for protein analysis, owing to their capabilities of achieving improved sensitivities (Dodeigne et al., 2000; Mathias et al., 2008). However, their drawbacks include the need for catalysts or enhancers, a long incubation time before reaching a stable output signal, the degradation of labels, and the use of expensive optical detectors and filters (Goldys, 2009; Lakowicz, 1999). An ideal biomarker-detection assay should offer high sensitivity, high specificity, low-cost instrumentation with high throughput, and long-term stability of the labels for future analysis.

The development of nanomaterials and nanoparticles during the past decade provides tremendous opportunities to address existing challenges in biomarker detection on a nanoscale (de la Escosura-Muniz et al., 2010; Huang et al., 2009; Segev-Bar and Haick, 2013). In particular, the interaction of light with a metal nanoparticle results in the collective oscillation of free electrons within the nanoparticle, which is known as localized surface plasmon resonance (LSPR). (Sagle et al., 2011; Willets and Van Duyne, 2007). LSPR is associated with a strongly localized and greatly enhanced evanescent field, which has been utilized in several areas of research, including photovoltaics, photocatalysis, biomolecule sensing, cell imaging, and photothermal therapy (Awazu et al., 2008; Cao et al., 2002; Govorov et al., 2006; Nam et al., 2003; Stratakis and Kymakis, 2013). Here, we utilized the photothermal effect of gold nanoparticles (AuNPs) to develop a new type of immunoassay, referred as the photoacoustic (PA)-

* Corresponding author at: 2128 Coover Hall, 2520 Osborn Dr., Ames, IA 50011, USA.
E-mail address: menglu@iastate.edu (M. Lu).

http://dx.doi.org/10.1016/j.bios.2016.05.028
0956-5663/© 2016 Elsevier B.V. All rights reserved.

immunoassay. AuNPs were chosen for three main reasons. First, AuNPs can effectively convert photons into heat owing to non-radiative resonant absorption. The strong photothermal effect of AuNPs has been successfully utilized to selectively kill target cells and to serve as a signal enhancer for photoacoustic tomography (Jaque et al., 2014; Yang et al., 2009). Second, surface AuNPs can be conjugated with various types of ligands that recognize target biomarkers with high specificity (Sperling and Parak, 2013). Third, owing to their excellent physical and chemical stabilities, AuNPs can generate reproducible signals. By quantifying the PA signal, which is directly proportional to the amount of AuNPs, the nanoparticle-based immunoassay enables a sensitive, repeatable, and inexpensive approach for analyzing biomarkers.

Since the mid-1970s, the PA detection has attracted considerable interest in the analytical community due to its capability of measuring optical absorption of samples in gaseous, liquid, and solid phases (McClelland and Kniseley, 1976; Rosencwaig, 1990). The PA detection method offers several compelling features. For example, PA measurements can be performed without difficulties in collecting and detecting photons, common to fluorescence and Raman spectroscopies; as a result, no expensive photodetectors or optical filters are required. The PA technique generates quantitative signals based on a 3-step process involving AuNP optical absorption, conversion of the absorbed energy into heat, and the subsequent heat-induced thermal expansion of the adjacent media, which produces pressure oscillations or propagating acoustic waves when the incident beam is modulated at an acoustic frequency. As illustrated in Fig. 1(a), the PA-based detection of an AuNP-labeled biomarker takes place inside a sealed sample chamber, which is relatively small compared to typical acoustic wavelengths used for PA measurements. A modulated laser beam is used as the excitation source to generate pressure oscillations, and a microphone is installed inside the sample chamber to measure the signal.

Here, we present the first demonstration of a PA-based immunoassay and a detection instrument devised for the assay. By investigating the PA signal with bare AuNPs coated on a plastic substrate, we validate PA measurements as a quantitative approach for detecting AuNPs. Next, a simple test protein (streptavidin) was used to shown the correlation between the PA signal and its concentration. As an example of a PA immunoassay, the PA-based approach was evaluated by analyzing detection of a chemokine biomarker (human interleukin 8 [IL-8]). The PA immunoassay improved the limit of detection (LOD) by approximately a factor of 143 compared with the ELISA method – a decrease from 23 pg/mL to 0.16 pg/mL.

The following sections of this report are as follows. Section 2 describes the experimental details of the PA immunoassay and the detection setup for the PA experiment. Section 3 presents the results of the PA detection of AuNPs, as well as the PA immunoassay used for detecting IL-8. Section 4 concludes this study and discusses future avenues of investigation with the PA immunoassay.

2. Material and methods

2.1. Materials and reagents

Biotin-conjugated gold nanorods and streptavidin-conjugated gold nanorods were purchased from Nanopartz, Inc. (Loveland, CO, USA). Polyvinylamine (PVAm; MW=340 kDa) was obtained from BASF (New Jersey, USA) and diluted in water to obtain a 5% solid solution, which was used as the surface-functionalization material. Glutaraldehyde (GA), bovine serum albumin (BSA), streptavidin (SA) protein, Tween-20, and phosphate buffered saline (PBS, 10 mM, pH=7.4) were purchased from Sigma-Aldrich (St. Louis, MO, USA). The Human IL-8 ELISA Kit was purchased from Thermo Fisher Scientific (Waltham, MA, USA). The kit contained a monoclonal mouse anti-human IL-8 antibody (capture antibody), a recombinant human IL-8 protein standard, a human IL-8 biotinylated antibody (detection antibody), horseradish peroxidase-conjugated SA (SA-HRP), tetramethylbenzidine (TMB) substrate, and stop solution (0.16 M sulfuric acid).

2.2. PA detection setup

The PA detection setup consisted of a frequency doubled Nd:YAG laser (λ=532 nm; P_{out}=50 mW), an optical chopper (SRS540, Stanford Research Systems), a PA detector (PAC 200, MTEC Photoacoustics, Inc.), and a data-acquisition device, as shown in Fig. 1 (b). The acrylic substrates were placed inside the PA chamber one at a time for PA measurements. After loading the sample, the chamber was sealed to eliminate ambient noises. For all PA measurements, the chopping frequency of the optical chopper was set at 13 Hz. The laser beam from the Nd:YAG laser passed though the optical chopper and a glass window in the PA chamber. The intensity-modulated laser beam was absorbed by the AuNPs on the acrylic substrate and caused periodic heating of the air inside the

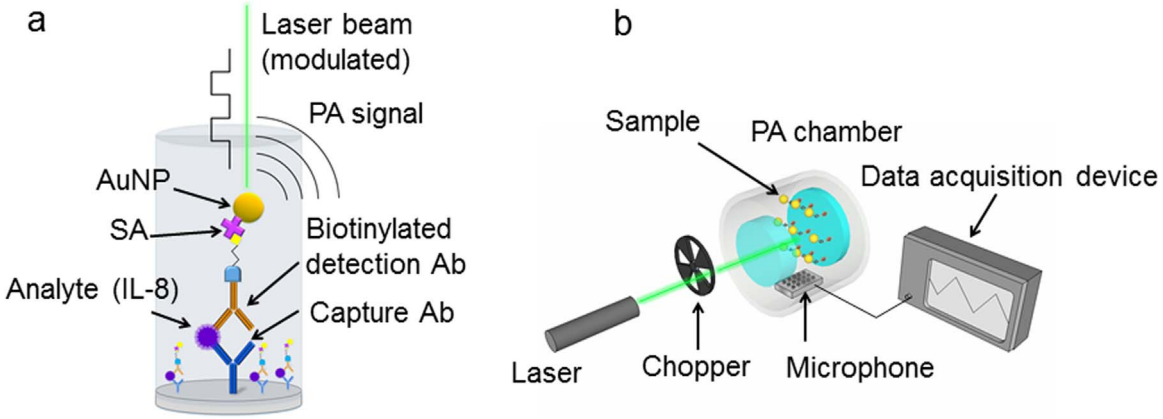

Fig. 1. (a) PA immunoassay format and (b) PA setup. During a PA measurement, a chopper is used as the modulator, which periodically blocks the laser at 13 Hz. The sample placed in a sealed chamber is periodically heated and, therefore, periodically expands and contracts, generating a pressure oscillation that is detected by the microphone and displayed as a waveform on an oscilloscope. A sandwich format is used for the immunoassay, wherein the analyte is immobilized by a capture antibody and tagged with a detection antibody, which is further tagged with a conjugated AuNP. The AuNPs generate a PA signal in the aforementioned setup, and the signal intensity reflects the concentration of the analyte.

PA chamber. The thermal expansion and contraction cycles resulted in pressure oscillations within the PA chamber. An acoustic transducer, i.e., a microphone (4176, Brüel & Kjær A/S), was connected to the chamber to measure PA pressure oscillations. The output of the microphone was amplified by a preamplifier integrated inside the PA-detection system and was subsequently measured using an oscilloscope (TDS2014B, Tektronix) or a lock-in amplifier (SRS-850 DSP, Stanford Research Systems).

2.3. SA protein-binding assay

To validate PA detection as an effective method for protein analysis, we developed a proof-of-concept assay to measure SA concentrations (MW = 52.8 kDa). Acrylic windows were chosen as the substrate, owing to their low thermal conductivity and low cost. SA molecules were immobilized on an acrylic substrate and labeled using biotin-conjugated AuNPs to generate PA signals. The initial step in the assay was to coat the acrylic substrates using PVAm, which provided high-density amine functional groups on the plastic substrate. For the second step, the substrates were soaked in GA solution (25% in water) for 3 h, followed by a thorough wash with de-ionized (DI) water. GA molecules covalently attached to the PVAm. As a bifunctional linker, the GA treatment enabled the capture of protein molecules via their amine moieties. The third step of the protocol was to capture SA samples on the substrates. A series of SA samples with various concentrations were prepared in PBS buffer. The SA samples (50 μL) were pipetted onto the acrylic substrates and incubated overnight, followed by 3 washes with PBS. Next, the unoccupied aldehyde functional groups were blocked by soaking the acrylic substrates in BSA solution (1 mg/mL) for 4 h, followed by a wash step. The final step of the assay was to label the immobilized SA using biotinylated AuNPs. The AuNP suspension was diluted to a concentration of 1×10^{12} NPs/mL and dispersed onto the acrylic substrates. After a 2-min incubation, the acrylic substrates were washed sequentially using DI with 0.05% Tween. The acrylic substrates were then dried under a stream of compressed air and placed in the measurement chamber for PA measurements.

2.4. Sandwich immunoassays for human IL-8 antigen

As an example of biomarker analysis, the human IL-8 antigen was chosen as the target molecule because of its clinical significance, as it is related to inflammation, obesity, and other diseases (Shahzad et al., 2010; Sharabiani et al., 2011). Two sets of human IL-8 dilution series were measured using ELISA and PA immunoassays, respectively. The major steps involved in the immuno-sandwich assays are summarized in Fig. 2. The assays were performed in a microtiter plate. The bottoms of the wells were coated with the IL-8 capture antibody and then blocked in a solution of BSA (1 mg/mL) in PBS for 1 h at room temperature. Colorimetric Standard curves were generated using a 2.5-fold dilution series of IL-8 antigen for a total of 7 antigen concentrations, from 1000 pg/mL to 4.096 pg/mL, and a blank (dilution buffer only). IL-8 samples (50 μL) were incubated in microtiter plates at room temperature for 1 h. The substrates were then washed in PBS with 0.05% Tween (PBS-T), followed by an incubation with biotinylated IL-8-detection antibodies at 25 ng/mL in PBS-T for 2 h. Then, PBS-T was used to wash the samples and remove excess detection antibodies. For the ELISA measurements, 100 μL of SA-HRP solution was added to each well for 30 min as the enzymatic label, followed by 3 washes with PBS-T. Next, 100 μL of TMB substrate was added into each microwell, after which the TMB underwent a colorimetric reaction catalyzed by the HRP molecules. After a 30-min development, the reaction was stopped by the addition of 100 μL of stop solution. The results were measured using a spectrophotometer (BioTek). To generate the standard curve, the difference between the absorbance at 450 nm and 550 nm was calculated for each antigen concentration.

For the PA-immunoassay (Fig. 2), the dilution series was extended down to 0.016 pg/mL and the detection antibody was labeled using SA-conjugated AuNPs, rather than the SA-HRP solution. After a 15-min incubation, the AuNP solution was removed, followed by 3 washes with PBS-T. Before the PA measurement, the

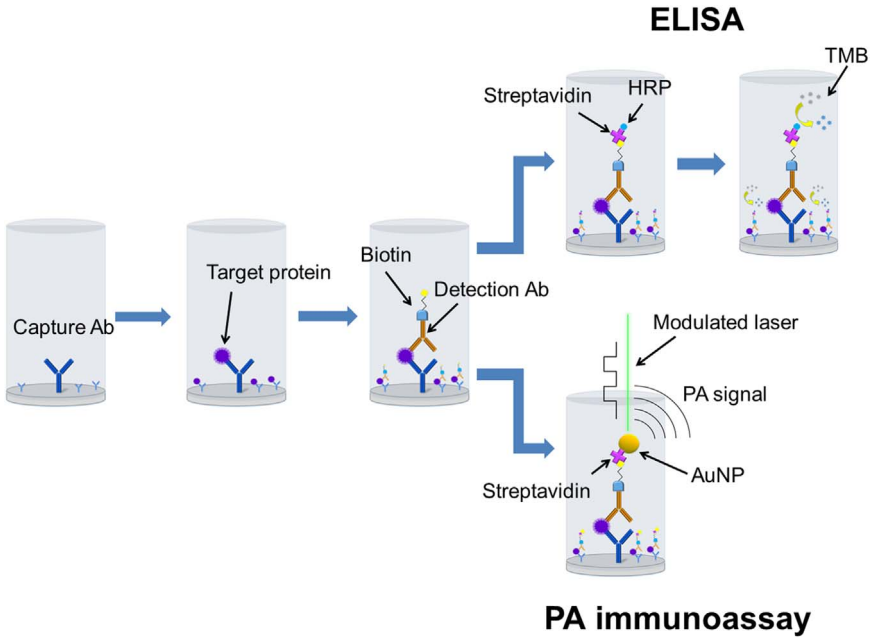

Fig. 2. Immuno-sandwich assay flow chart. The upper branch shows the colorimetric ELISA flow chart. The analyte, biotinylated detection Ab, SA-HRP, and TMB substrate are sequentially added to the microtiter well, whose bottom was pre-treated with the capture Ab. At the assay endpoint, a stop solution is added to stop the colorimetric reaction, and the color of the final product reflects the analyte concentration. The lower branch shows the PA immunoassay. The SA-HRP in the colorimetric ELISA is replaced with an SA-conjugated AuNP, and the TMB substrate is not used. The AuNPs are bound to an antigen-antibody complex. Measuring the PA signal of AuNPs enables determination the analyte concentration. (For interpretation of the references to color in this figure legend, the reader is referred to the web version of this article.)

samples were dried in air at room temperature.

2.5. Numerical simulation

Finite difference time domain (FDTD) simulations were performed to characterize the optical responses of AuNPs on an acrylic substrate. FDTD simulation can be used to calculate the extinction spectrum and the near-field distribution at a spectral location for metal nanoparticles illuminated by the resonance wavelength (Tira et al., 2014). In this work, the simulation domain included a single AuNP located on the surface of a flat polymer substrate. The optical properties of Au and acrylic substrate were taken from Palik's Handbook. The AuNP was illuminated with a plane wave propagating in the *z*-direction with the electric field polarized along the *x*-axis. The simulation region was truncated with periodic boundary conditions in the *x*- and *y*-directions, with perfectly matched layer boundary conditions in the z direction. Monitors were placed in close proximity to the boundaries to calculate the amount of reflected and transmitted power as a function of wavelength. A uniform fine mesh size of 1 nm (*x*-, *y*-, and *z*- directions) was used around the AuNP region.

3. Results

3.1. Simulation of surface plasmon resonance with AuNPs

To generate a strong PA signal with AuNPs, the emission wavelength of the excitation laser should match the LSPR wavelength of the AuNPs. The LSPR of a single AuNP placed on top of a flat plastic substrate was numerically determined using FDTD simulation. The AuNPs used in this study had an axial diameter of 8 nm and a length of 12 nm and were immobilized at the air-substrate interface. The absorption spectrum of the single AuNP is shown in Fig. 3(a), where the resonance peak was located at approximately 553 nm. At the resonance wavelength, the AuNP strongly absorbed the incident light and resulted in efficient heating of the surrounding air. To maximize the heating effect, a frequency doubled Nd:YAG laser ($\lambda = 532$ nm), whose wavelength was close to the resonance wavelength, was chosen as the excitation source. At the resonance wavelength, the near-field distribution across the AuNP was calculated, as shown in Fig. 3(b), where the pseudo-color map represents the electric field intensity relative to the intensity of the incident field. The white line and the black ellipse indicate the surfaces of the plastic substrate and the AuNP, respectively. As shown, LSPR occurring in close vicinity to the AuNPs enhanced the near electric field by a factor of over 90-fold. The associated enhancement of optical absorption led to very strong heat generation that boosted the photothermal and photoacoustic effects.

3.2. Measurement of AuNPs using PA detection

After identifying an optimal excitation wavelength, we performed a preliminary study of PA quantification of AuNPs absorbed on an acrylic substrate to demonstrate the feasibility of PA detection as an analytic method for plasmonic NPs. For this experiment, 7 AuNP suspensions were prepared by generating a dilution series, with AuNP concentrations of 1.0×10^{12}, 3.3×10^{11}, 1.0×10^{11}, 3.3×10^{10}, 1.0×10^{10}, 3.3×10^{9}, and 1.0×10^{9} NPs/mL. The AuNP samples (50 μL) were pipetted onto the acrylic substrates and air-dried before PA measurements were taken. Fig. 4 shows the PA signals measured using an oscilloscope, as well as their fit to a logistic curve. The PA signal increased with the AuNP concentration. At lower concentrations, the PA signal showed a linear correlation with the AuNP concentration. At higher concentration levels, the PA signal became saturated. The noise level of these measurements was limited by the PA signal of the acrylic substrate (30 mV).

3.3. Measurement of SA using PA detection

As a proof-of-concept to demonstrate the utility of protein analysis using the PA method, a PA-based assay for the detecting SA was developed. To this end, PVAm-GA and biotinylated AuNPs were used as the SA receptor and the label, respectively. As shown in Fig. 5(a), SA immobilization occurred on the PVAm- and GA-coated acrylic substrate. Then, SA samples were added to the substrates, using a series of SA concentrations (100, 25, 6.25, 4, 2, 0.8, or 0 μg/mL). The captured SA molecules were labeled using biotinylated AuNPs (1.0×10^{12} NPs/mL) through avidin-biotin binding, and thus, the PA signal generated by the AuNPs represented the SA concentration. The PA signals of the SA samples are shown in Fig. 5(b). The linear range of the detection was in the range of 2–25 μg/mL. The PA signal approached saturation at an SA concentration of 100 μg/mL. The LOD of the SA (1.2 μg/mL) was calculated as the PA background signal of the acrylic substrate plus 3 times its standard deviation. These results demonstrated the feasibility of the PA-based approach for protein quantification.

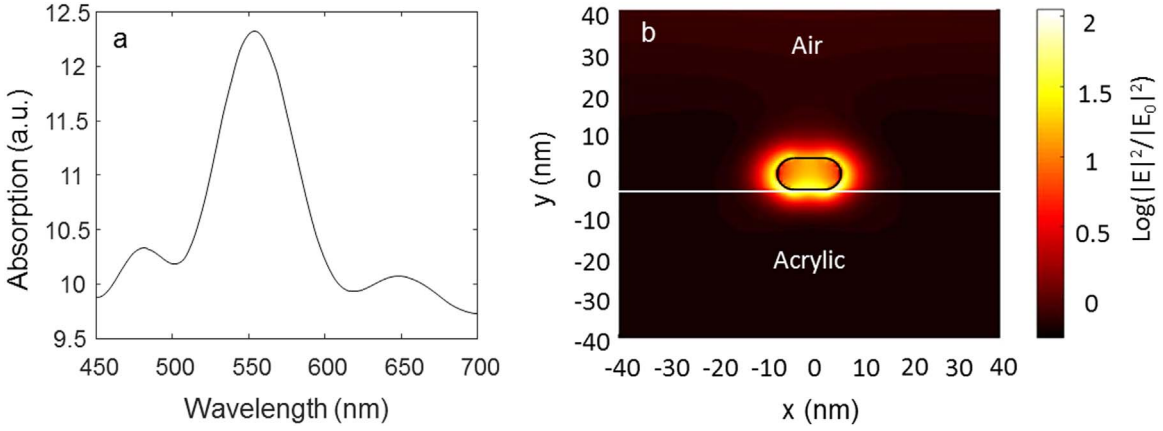

Fig. 3. (a) FDTD simulation of the absorption spectrum of an AuNP on an acrylic substrate. (b) The electrical field distribution was calculated at a cross section of the AuNP. At the LSPR resonance (near 550 nm), the local electrical field ($\boldsymbol{E}_0$) showed a 90-fold enhancement relative to that of the excitation alone. (For interpretation of the references to color in this figure, the reader is referred to the web version of this article.)

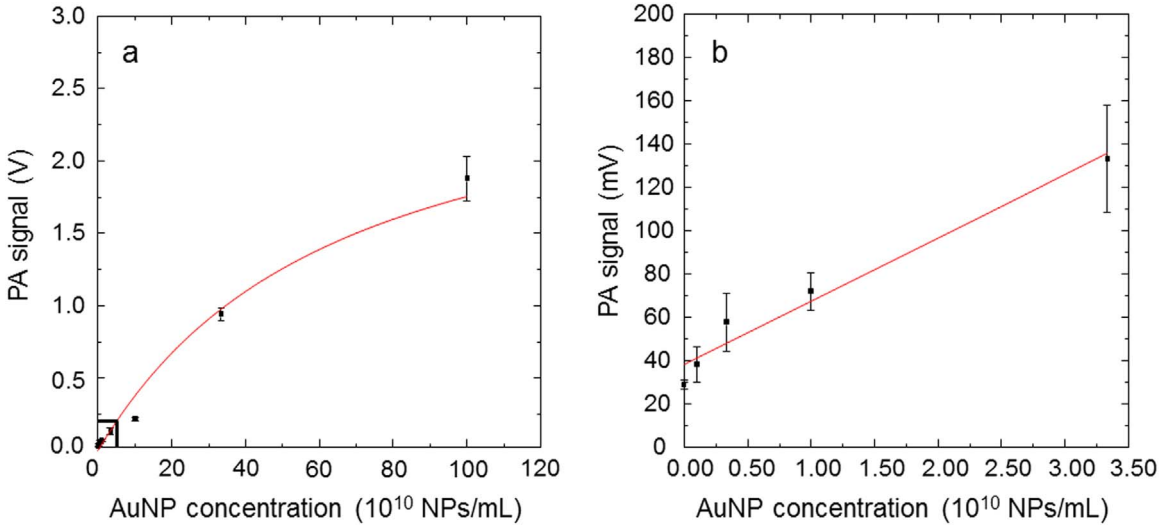

Fig. 4. PA signal plotted as a function of the AuNP concentration. (a) PA signals of samples at high concentrations. The PA signal approaches saturation when the AuNP concentration was increased to 1.00×10^{12} NPs/mL. (b) PA signals of samples at low concentrations denoted by the box in (a). The PA signal showed a linear relation with respect to the AuNP concentration. The PA signal of the acrylic substrate was 30 mV.

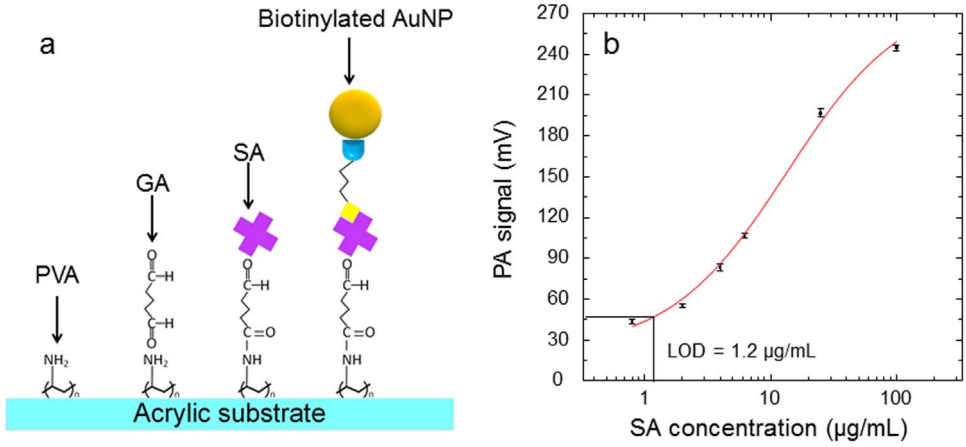

Fig. 5. (a) Schematic representation of the SA-measurement assay. SA was immobilized on an acrylic substrate pre-treated with PVAm and GA, after which it was labeled with biotinylated AuNPs. (b) PA signal plotted against the SA concentration. The LOD was measured as 1.2 μg/mL.

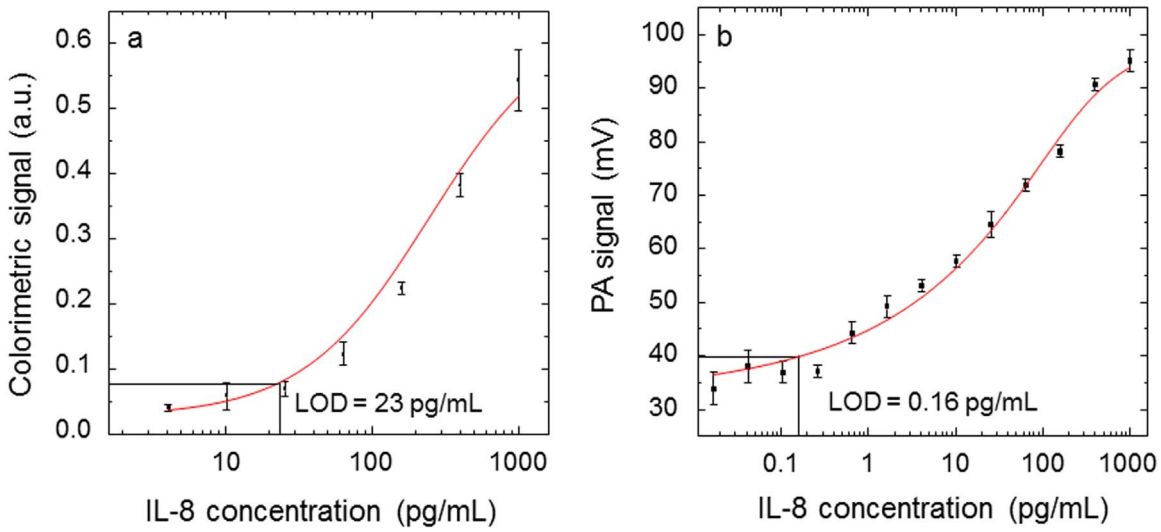

Fig. 6. (a) Colorimetric results of the ELISA test for human IL-8. The colorimetric results were calculated based on differences between the optical densities at 450 nm and 550 nm. The data points were fitted using a logistic regression. The LOD of the ELISA measurement was calculated as 23 pg/mL. (b) IL-8 titration curve generated using the PA immunoassay. The PA immunoassay showed a lower LOD (0.16 pg/mL) than did the ELISA.

3.4. Detection of human IL-8 antigen using the PA immunoassay

To determine the performance of the PA immunoassay, the detection of a chemokine protein, human IL-8, was performed using the PA-immunoassay and the results were compared with those of the colorimetric ELISA. To generate a titration curve for IL-8, we prepared IL-8 samples at a series of 13 concentrations ranging from 1000 pg/mL to 0.016 pg/mL, with 2.5-fold dilutions. The colorimetric signals of the ELISA tests were measured using a spectrophotometer. Fig. 6(a) shows the measured optical density as a function of the IL-8 concentration. The PA signals of the PA immunoassay test were measured using an MTEC detector and a lock-in amplifier. The lock-in amplifier effectively reduces random noise generated by the electronic components. The titration curve of the PA immunoassay is shown in Fig. 6(b). The LOD of the PA immunoassay was approximately 0.16 pg/mL, which represents an improvement of more than two orders of magnitude compared with the ELISA result of 23 pg/mL.

According to clinical evaluations of serum IL-8 levels in healthy adults, the physiology concentration of IL-8 is approximately 30 pg/mL (Kleiner, 2013), which just within the LOD capability of ELISA serum analyses, but the PA immunoassay developed in this study provides a lower LOD capability applicable to diseases such as bladder cancer. Data from a recent study suggested that the IL-8 secretion level is increased in patients with invasive bladder cancer, making IL-8 a potential biomarker for bladder cancer screening (Urquidi et al., 2012). Urine analysis showed that the IL-8 concentration increased from 0 pg/mL to 128.43 pg/mL in samples from patients with bladder cancer. The sensitivity of the PA immunoassay for IL-8 detection is sufficiently high to enable accurate IL-8 determinations in either serum or urine samples.

4. Discussion and conclusions

In summary, to facilitate biomarker detection, we developed the PA immunoassay as a highly quantitative, sensitive, robust, and inexpensive analysis platform. The PA immunoassay can be used to quantify biomarkers, based on acoustic waves that are generated by the AuNP labels. The rationale for this approach lies in the advantages associated with efficient energy conversion that is enabled by the plasmonic nanoparticles, as well as the accuracy and simplicity of measuring acoustic signals. The use of photoacoustic detection also eliminates various types of noise, such as the leakage of excitation light through optical filters and the autofluorescence of commonly used materials, which can deteriorate the performance of most photon-based detection systems. The PA immunoassay was based upon the standard sandwich immunoassay, with AuNPs being used as the labeling material. An intensity-modulated laser beam at 532 nm was used to excite PA signal and the samples were measured in a sealed chamber. The PA-immunoassay results for human IL-8 detection demonstrated that the PA approach had significantly improved assay sensitivity (>2 orders of magnitude), compared to ELISA results (LODs of 0.16 pg/mL and 23 pg/mL, respectively). In addition to improved LOD, the PA immunoassay also offers advantages in terms of signal stability and simplicity. The colorimetric signal of ELISA samples must be measured within 30 min after adding the stop solution. The plasmon-enhanced fluorescence assay needs both fluorescence tags and metal nanoparticles, and the bleaching and quenching problems affect the fluorescence output. In contrast, the PA immunoassay only relies on the AuNPs to generate the output signal. The results of the PA immunoassay are stable over a long period of time, and multiple measurements can be taken without introducing problems such as bleaching or signal degradation.

The PA immunoassay is currently at an early stage, and has great potential for further development. The PA immunoassay would be improved by further increasing the signal-to-noise ratio. This can be achieved by increasing the laser power to generate a stronger PA signal, optimizing the design of the PA chamber to better suit the purpose of PA immunoassay, or using a compact microphone array to better collect the PA signal. Other means to improve the PA immunoassay would be to miniaturize the PA detection setup and to integrate the light source, PA chamber, and data acquisition and display into a single device that enables PA analysis for point-of-care testing. It may also be possible to reduce the LOD by reducing the background signal from the substrate and sample chamber. In addition, the PA immunoassay could be implemented using most existing protein-analysis formats, such as lateral and vertical flow assays, to become a versatile analytic tool.

Acknowledgements

This research was supported by startup funding from Iowa State University and the 3M Non-Tenured Faculty Award.

References

Awazu, K., Fujimaki, M., Rockstuhl, C., Tominaga, J., Murakami, H., Ohki, Y., Yoshida, N., Watanabe, T., 2008. J. Am. Chem. Soc. 130 (5), 1676–1680.
Cao, Y.C., Jin, R., Mirkin, C.A., 2002. Science 297 (5586), 1536–1540.
de la Escosura-Muniz, A., Parolo, C., Merkoci, A., 2010. Mater. Today 13 (7–8), 17–27.
Dodeigne, C., Thunus, L., Lejeune, R., 2000. Talanta 51 (3), 415–439.
Fan, R., Vermesh, O., Srivastava, A., Yen, B.K.H., Qin, L.D., Ahmad, H., Kwong, G.A., Liu, C.C., Gould, J., Hood, L., Heath, J.R., 2008. Nat. Biotechnol. 26 (12), 1373–1378.
Gan, S.D., Patel, K.R., 2013. J. Invest. Dermatol. 133 (9), e12.
Goldys, E.M., 2009. Fluorescence Applications in Biotechnology and Life Sciences. John Wiley & Sons, Hoboken, N.J.
Govorov, A.O., Zhang, W., Skeini, T., Richardson, H., Lee, J., Kotov, N.A., 2006. Nanoscale Res. Lett. 1 (1), 84–90.
Hanash, S.M., Baik, C.S., Kallioniemi, O., 2011. Nat. Rev. Clin. Oncol. 8 (3), 142–150.
Hecht, A., Kumar, A.A., Kopelman, R., 2011. Anal. Chem. 83 (18), 7123–7128.
Huang, C.S., George, S., Lu, M., Chaudhery, V., Tan, R., Zangar, R.C., Cunningham, B.T., 2011. Anal. Chem. 83 (4), 1425–1430.
Huang, X.H., Neretina, S., El-Sayed, M.A., 2009. Adv. Mater. 21 (48), 4880–4910.
Jaque, D., Maestro, L.M., del Rosal, B., Haro-Gonzalez, P., Benayas, A., Plaza, J.L., Rodriguez, E.M., Sole, J.G., 2014. Nanoscale 6 (16), 9494–9530.
Kleiner, G., Marcuzzi, A., Zanin, V., Monasta, L., Zauli, G., 2013. Mediat. Inflamm., 2013.
Lakowicz, J.R., 1999. Principles of Fluorescence Spectroscopy, second ed. Kluwer Academic/Plenum, New York.
Lequin, R.M., 2005. Clin. Chem. 51 (12), 2415–2418.
Ludwig, J.A., Weinstein, J.N., 2005. Nat. Rev. Cancer 5 (11), 845–856.
Mathias, P.C., Ganesh, N., Cunningham, B.T., 2008. Anal. Chem. 80 (23), 9013–9020.
McClelland, J.F., Kniseley, R.N., 1976. Appl. Opt. 15 (11), 2658–2663.
Nam, J.M., Thaxton, C.S., Mirkin, C.A., 2003. Science 301 (5641), 1884–1886.
Rhea, J.M., Molinaro, R.J., 2011. Med. Lab. Obs. 43 (3), 10–12 16, 18; Quiz 20, 22.
Rosencwaig, A., 1990. Photoacoustics and Photoacoustic Spectroscopy. R.E. Krieger Pub. Co., Malabar, Fla.
Sagle, L.B., Ruvuna, L.K., Ruemmele, J.A., Van Duyne, R.P., 2011. Nanomedicine 6 (8), 1447–1462.
Segev-Bar, M., Haick, H., 2013. ACS Nano 7 (10), 8366–8378.
Shahzad, A., Knapp, M., Lang, I., Kohler, G., 2010. Int. Arch. Med. 3, 11.
Sharabiani, M.T.A., Vermeulen, R., Scoccianti, C., Hosnijeh, F.S., Minelli, L., Sacerdote, C., Palli, D., Krogh, V., Tumino, R., Chiodini, P., Panico, S., Vineis, P., 2011. Biomarkers 16 (3), 243–251.
Sperling, R.A., Parak, W.J., 2013. Ther. Innov. Regul. Sci. 47 (1), 1333–1383.
Stratakis, E., Kymakis, E., 2013. Mater. Today 16 (4), 133–146.
Tira, C., Tira, D., Simon, T., Astilean, S., 2014. J. Mol. Struct. 1072, 137–143.
Urquidi, V., Chang, M., Dai, Y.F., Kim, J., W1olfson, E.D., Goodison, S., Rosser, C.J., 2012. BMC Urol. 12 (1), 1.
Voller, A., Bartlett, A., Bidwell, D.E., 1978. J. Clin. Pathol. 31 (6), 507–520.
Willets, K.A., Van Duyne, R.P., 2007. Annu. Rev. Anal. Chem. 58, 267–297.
Yang, X.M., Stein, E.W., Ashkenazi, S., Wang, L.H.V., 2009. Wires Nanomed. Nanobiotechnol. 1 (4), 360–368.
Yingyongnarongkul, B.E., How, S.E., Diaz-Mochon, J.J., Muzerelle, M., Bradley, M., 2003. Comb. Chem. High. Throughput Screen. 6 (7), 577–587.